The 14th IFToMM World Congress, Taipei, Taiwan, October 25-30, 2015
DOI Number: 10.6567/IFToMM.14TH.WC.OS20.021

Thermal Analysis of an Extrusion System of a 3-D Bioprinter

G. S. Ribeiro[1]
University of Sao Paulo
Sao Carlos, Brazil

J. V. L. Silva
CTI
Campinas, Brazil

D. Freitas
University of Manchester
Manchester, United Kingdom

P. Bártolo
University of Manchester
Manchester, United Kingdom

H. Almeida
CDRSP
Leiria, Portugal

Z. C. Silveira [2]
University of Sao Paulo
Sao Carlos, Brazil

Abstract: *This work presents a finite element thermal analysis of a 3-D bioprinter desktop based on Fused Deposition Modeling (FDM) with applications on tissue engineering, designed by the Centre for Rapid and Sustainable Product Development – Leiria, Portugal. The purpose of this work it is compare three possibilities of temperature control of the machine during the extrusion process, considering the use of a biodegradable polyester (Polycaprolactone - PCL) as raw material. The first two configurations simulate approaches typically adopted in an attempt to keep the polymer as close as possible to 80 °C and prevent its premature solidification at a critical point. The third configuration considers a hypothetical material substitution to enhance thermal conductivity. The results indicate that the first two configurations are not sufficient to achieve total control of the polymer temperature. However, the third configuration show a significant potential to improve the thermal control of the extrusion process.*

Keywords: heat transfer, finite element modeling, 3-D printer, biopolymer, extrusion process.

I. Introduction

The development of biological and anatomical models was one of the first and most important approaches that lead the Additive Manufacturing (AM) technologies into biomedical field. In addition to the development of models for surgical training and planning, the direct manufacture of customized implantable medical devices has been, in the past two decades, another main bioengineering area at which AM technologies have been used. However, it is important to pay close attention to aspects such as standardization and quality control in order to obtain completely safe products for the patients.

Bioengineering is the biological or medical application of engineering principles or engineering equipment, also called biomedical engineering. One of its most recent subfield is the tissue engineering, which is an interdisciplinary field of research that combines cell biology, engineering, material science, mathematics and genetics aiming to develop biological substitutes that restore maintain or improve tis-sue functions [1].

Scaffolds are structures that provide an initial biochemical substrate for a novel tissue growth until cells can produce their own extra-cellular matrix (ECM). In addition, provide the appropriate function to its tissues. Scaffolds must be an open porous structure, filling the deficient tissue and enabling tissue ingrowth [1]. For the repair and generation of hard and ductile tissues, scaffolds need to have a high elastic modulus and provide to the tissue the proper space for the growth [2].

The conventional techniques for scaffold fabrication include fibre bonding, solvent casting, particulate leaching, membrane lamination, melt moulding and solid freeform fabrication (SFF) techniques, like 3D printing [2]. It is worth noting that the technology of 3D printing was originally designed to create prototypes; therefore, few efforts have been made to improve the manufacturing process of scaffold samples [3]. However, SFF has shown to be highly effective in integrating structural architecture with changes in surface chemistry [4].

Among several requirements of an ideal scaffold design, the pore size is the responsible to guarantee the successful diffusion of essential nutrients and oxygen for cell viability, where at least a 100 μm diameter is required. For example, in bone tissue in-growth, pore sizes in the range of 200 to 350 μm are found to be optimum. However, scaffolds with non-uniform porosity are useful, since the natural bones does not have a uniform distribution of porosity [5]. Another example about this topic concerns cartilage regeneration. Using collagen porous scaffold with spherical pore structures with good interconnectivity, which had it best pore diameter in the range of 150 to 250 μm in a comparative study [6].

Besides other properties, scaffolds must have always the proper geometric characteristics, such as shape and pore size, in a constant attempting to better biomimicry. Only interdisciplinary approaches at multiple length scales can direct to an effective optimization of this field of study [5].

3D printing technology has found several applications since its conception, such as printing proto-types, medical implants, fashion industry, military applications and others. The original design is drafted (or enhanced) in a CAD program, which is converted to the .STL file format, developed by 3D Systems, storing in triangulated sections information about each surface of the 3D model. Then, the 3D printer can interpret the coordinates of triangles vertices by converting the supplied file into a G-file via a slicer software. By dividing the 3D .STL file into a sequence of two-dimensional horizontal cross sections, it allows the object to be printed, layer by layer, positioning its deposition nozzle into a plane surface [7].

In a mechanical point of view, tissue engineering will always benefit from the improvement of the ability to position large quantities of cells and biomaterials within a three-dimensional volume in a reasonable timeframe [8]. For this, it is necessary to keep in mind the cost of a new design. A way of introducing the concept of 3D printing in

[1]gustavo.santos.ribeiro@usp.br
[2]silveira@sc.usp.br

low-cost desktop conventional printers is to design new heads for it. By changing the way of work of a head, it is possible to introduce a very different concept to the manufacturing process. In this aspect, the most usual technologies applied to desktop 3D are Fused Deposition Modeling (FDM) and extrusion by a syringe.

However, several new technologies are being developed. For example, Pepper, et al. [8] described the capability of using a HP26 series print cartridge modified to work with a cell solution, also known as "bio-ink". Inforçatti, et al. [9] have developed an interchangeable extrusion head based on variable section screw, applied to desktop 3D printers, which was successful tested in an open source model. In addition, Mironov, Kasaynov and Markwald [10] explore future challenges regarding to the creation of a fully integrated organ bio fabrication line, and state that further progress in bioprinter development must focus on improving nozzle and cartridge design.

This work is about another concept that is being developed, using a new design of extrusion head allied to the pursuit of an equally relevant machine shape and structure. By better understanding the basic thermal behavior of the machine, it can be possible to achieve new perspectives that will help in the configuration of an optimized process.

II. Background

A. *Biocompatible polymers*

Polycaprolactone (PCL) is a biodegradable polymer in the field of bioengineering due to its mechanical properties, miscibility with other polymers and, mostly, due to its biodegradability properties [11].

The commercial product fed to the machine during the study was Capa™6500, a high molecular weight thermoplastic linear polyester derived from caprolactone monomer, supplied in granular form (pellets). Its properties are listed in Table 1.

Properties	Range	Ref.
Density, g/cm^3	1.071 to 1.200	[11, 24]
Elongation at break, %	800	[11]
Glass transition temperature, ºC	(-65) to (-60)	[11, 13]
Mean molecular weight, g/mol	50 000	[24]
Melting point, ºC	58-60	[24]
Thermal conductivity, W/m.K	0,25	[23, 25]

Table 1 – CapaTM6500 properties.

The value of the mean molecular weight shown in Table 1 is related to an entire carbonic chain. The molecular weight of the repeated unit of the PCL is $114.15\ g/mol$ [12]. In addition, Gaur, et al., [13] have compiled a series of papers containing the heat capacity measurements of the most important linear macromolecules. From values that ranges from $0.0\ J/mol\ K$ for $0.0\ K$ to $120.9\ J/mol\ K$ for $209.0\ K$ (Glass transition temperature), considering the semicrystalline state, and then from $181.1\ J/mol\ K$ for $209.0\ K$ to $221.6\ J/mol\ K$ for $350.0\ K$, considering the molten state, the eighth publication of this series gives us a complete table of heat capacities in a practical range of temperatures. These values are shown in a graph in Fig. 1.

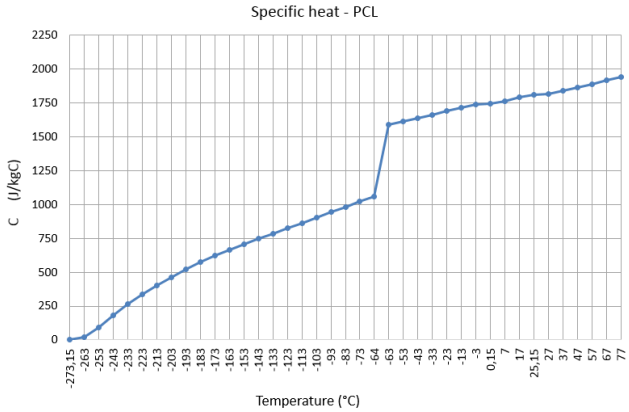

Fig. 1. Heat capacity versus temperature measured for the PCL, plotting from the table compiled [13].

B. *Equations of heat transfer*

Considering a general case, the Fourier's heat conduction equation can be written Eq. (1) [14]:

$$\begin{Bmatrix} f_x \\ f_y \\ f_z \end{Bmatrix} = -\boldsymbol{K} \begin{Bmatrix} \partial T/\partial x \\ \partial T/\partial y \\ \partial T/\partial z \end{Bmatrix} \quad (1)$$

where $\boldsymbol{K}$ is the thermal conductivity matrix, in general a full 3 by 3 matrix of thermal conductivities, f_x, f_y and f_z are the conduction heat flux per unit of area in x, y and z directions.

The Newton's law of cooling describes the convective heat transfer, given by Eq. (2) [15]:

$$f = \bar{h}(T_s - T_f) \quad (2)$$

where f refers to the convective heat flux per unit of area normal to the surface, T_s and T_f are the surface and surrounding fluid temperature, respectively. The term $\bar{h}$ refers to the average convection coefficient, defined as illustrated in Eq. (3):

$$\bar{h} = \frac{1}{A_s}\int_{A_s} h dA_s \quad (3)$$

The amount of energy emitted due to radiation by a surface, obtained from Stefan-Boltzmann law is represented by Eq. (4):

$$f = \varepsilon \sigma T_s^4 \quad (4)$$

Where f is the radiated heat flux, ε is the emissivity defined as the ratio of total emissive power of an ideal radiator at same temperature, σ is the Stefan-boltzmann's constant.

Consider the condition of gray-diffuse bodies. Gray body is a condition that assumes no dependence of radiation on wavelength. In this case, we have the equality

of ε and absorptivity α, which is related to ratio of total absorbed energy compared to that absorbed by a blackbody [15]. The diffuse condition assumes that ε and α do not depend on direction.

Extending the Stefan-Boltzmann Law for a system of N enclosures of gray-diffuse bodies, the energy balance for each surface in the enclosure is presented by Siegel and Howel [16], which relates the energy losses to the surfaces temperatures:

$$\sum_{i=1}^{N}\left(\frac{\delta_{ji}}{\varepsilon_i}-F_{ji}\frac{1-\varepsilon_i}{\varepsilon_i}\right)f_i=\sum_{i=1}^{N}(\delta_{ji}-F_{ji})\sigma T_i^4 \qquad (5)$$

Where:

N = number of radiating surfaces;
δ_{ji} = Kronecker delta;
ε_i = effective emissivity of surface i;
F_{ji} = radiation view factors;
f_i = energy loss of surface i per unit of area;
σ = Stefan-Boltzmann constant;
T_i = absolute temperature of surface i.

The conservation of energy in terms of heat transfer is given by Eq. (6):

$$q"A_i+E_{gen}-(q"_{conv}+q"_{rad})A_j=\rho c_p\frac{\partial T}{\partial t} \qquad (6)$$

C. *Considerations on finite element method in thermal analysis*

According to Cook [14], the use of finite elements method to solve problems related to heat transfer involves the calculation of temperatures within a solid body. A by-product of temperature calculation is the information on the magnitude and direction of the heat flow in the body. Heat is transferred to or from a body by convection and radiation and the heat flow across a boundary is analogous to surface load in stress analysis. A distributed internal heat source is similar to body force in stress analysis. At some points on the boundary or within temperatures can be calculated. These temperatures are equivalent to displacements in stress analysis.

Heat moves within the body by conduction. For a steady-state (time-independent) problem, the global finite element equation is given by:

$$\boldsymbol{K}_T\boldsymbol{T}=\boldsymbol{Q} \qquad (7)$$

Where matrix $\boldsymbol{K}_T$ depends on the conductivity of the material, $\boldsymbol{T}$ is a vector of node point temperatures of the solid body, and $\boldsymbol{Q}$ is a vector of thermal loads. The convection and radiation boundary conditions can contribute in terms of $\boldsymbol{K}_T$ and $\boldsymbol{Q}$. The problem focuses on solving unknown nodal temperatures in $\boldsymbol{T}$.

The formal approach to obtain the stiffness matrix of a displacement-based finite element begins by the interpolation of the temperature over an element from element nodal temperature ($\boldsymbol{T_e}$), given by equation (8):

$$T=[N_1N_2\ldots N_n]\begin{Bmatrix}T_1\\T_2\\\vdots\\T_n\end{Bmatrix}\ or\ T=\boldsymbol{N}\,\boldsymbol{T_e} \qquad (8)$$

Individual shape functions in $\boldsymbol{N}$ are suited to the element type. The form of interpolation determines the complexity of the temperature field that an element can represent. In Cartesian coordinates, temperature gradients element can be represented by equation (9):

$$\begin{Bmatrix}\frac{\partial T}{\partial x}\\\frac{\partial T}{\partial y}\\\frac{\partial T}{\partial z}\end{Bmatrix}=\begin{bmatrix}\frac{\partial N_1}{\partial x}&\frac{\partial N_2}{\partial x}&\cdots\frac{\partial N_n}{\partial x}\\\frac{\partial N_1}{\partial y}&\frac{\partial N_2}{\partial y}&\cdots\frac{\partial N_n}{\partial y}\\\frac{\partial N_1}{\partial z}&\frac{\partial N_2}{\partial z}&\cdots\frac{\partial N_n}{\partial z}\end{bmatrix}\begin{Bmatrix}T_1\\T_2\\\vdots\\T_n\end{Bmatrix} \qquad (9.a)$$

Or

$$\boldsymbol{T}_\partial=\boldsymbol{B}\boldsymbol{T}_e \text{ where } \boldsymbol{B}=\begin{Bmatrix}\partial/\partial x\\\partial/\partial y\\\partial/\partial z\end{Bmatrix}\boldsymbol{N} \qquad (9.b)$$

The equation for an element considering the conductivity matrix can be expressed by equation (10):

$$\boldsymbol{k}_T=\int\boldsymbol{B}^T\boldsymbol{k}\boldsymbol{B}dV \qquad (10)$$

where $\boldsymbol{k}$ is the array of thermal conductivities.

When steady-state conditions does not prevails, temperature change in a unit of volume of the material is computed by "thermal mass" that depends on the mass density (ρ) of the material and its specific heat (c). The equation (7) is changed to the:

$$\boldsymbol{K}_T\boldsymbol{T}+\boldsymbol{C}\dot{\boldsymbol{T}}=\boldsymbol{Q}\quad \text{where}\quad \boldsymbol{Q}=\boldsymbol{Q}(t) \qquad (11)$$

In which $\boldsymbol{T}=\partial\boldsymbol{T}/\partial t$. Matrix $\boldsymbol{C}$ can be called a "heat capacity" matrix, where:

$$\boldsymbol{C}=\sum\boldsymbol{c}\qquad \text{where}\qquad \boldsymbol{c}=\int\boldsymbol{N}^T\boldsymbol{N}\rho cdV \qquad (12)$$

III. Case Study

The Bioextruder present in Fig. 3, is an additive bio manufacturing system under development for tissue engineering applications, designed and assembled at the CDRSP – Centre for Rapid and Sustainable Product Development, located in Leiria, Portugal. It is a highly reproducible and low-cost system, enabling the controlled definition of several parameters, such as scaffold porosity in order to modulate mechanical strength and molecular diffusion, as well the fabrication of multi-material parts [17, 18].

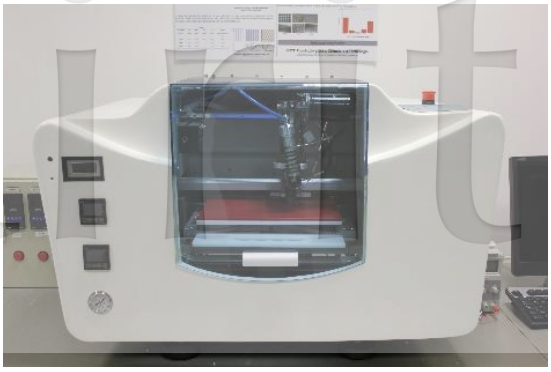

Fig. 2. Bioextruder developed in CDRSP-Leiria, Portugal

The extrusion system (Fig. 3) consists of an aluminum material deposit coated with an electrical resistance under the action of compressed air that allows the passage of material into a path, equally heated by an electrical resistance zone. At the base of the extrusion body, which is inserted the screwdriver, lies the extrusion nozzle that can be easily replaced depending on the desired dimensions of the filament. The stainless steel screw has a length of 50 mm, 10 mm diameter and 7 mm pitch, being driven by a DC motor. The maximum rotational speed of the screw is 90 rpm. The stainless steel extrusion nozzles are made with syringe nozzles and their dimensions range from 0.2 to 1 mm. An adapter makes the fastening system of the nozzles to the extrusion body. A board that allows adjustment of various parameters controls the spindle drive motor [19].

In a previous work related to the research of operational reliability of the machine, optimal parameters for the extrusion process were estimated when considering the polycaprolactone polymer CAPA^{TM}6500, as the base material. Among several other parameters, the optimal resistances temperature were set at 80º C [20]. However, over time this value proved that it was not very suitable for machine configuration due to certain factors, leaving open the possibility of exploring new thermal settings.

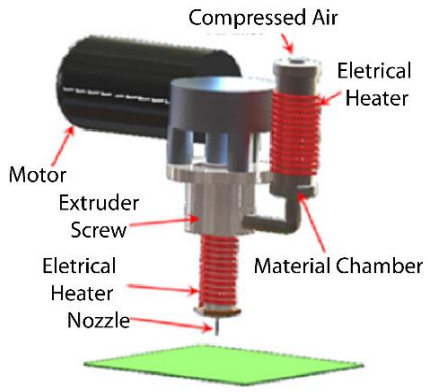

Fig. 3. Original design of the extrusion system [17].

IV. Numerical Analysis

A CAD model was created with maximum reliability and dimensional details as possible, so that it could be simplified in accordance with the analysis requirements, as shown in Fig. 4. Meanwhile, Fig. 5 shows the level of detail considered to the internal parts of the extrusion head, where all cavities were filled with a geometry that could represent the volume occupied by PCL during a regular extrusion process.

The next step was to define the critical subassembly for this analysis and to perform the generation of its finite element analysis (FEA) model, using ANSYS v 15.0. It is composed of an appropriate finite element mesh combined with boundary conditions to define the constraints for calculation (

Fig. 6). In this study, all model surfaces are subject to the effect of convection, represented by the letter "A" in the figure. The average convection coefficient $\bar{h}$ was setting as 2 $Wm^{-2}K^{-1}$, related to the natural convection heat transfer for heated plate facing upward [21].

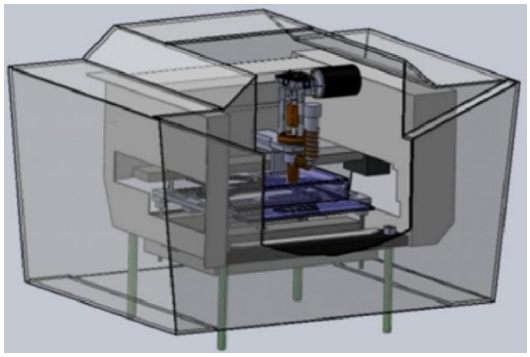

Fig. 4. CAD model representing the Bioextruder.

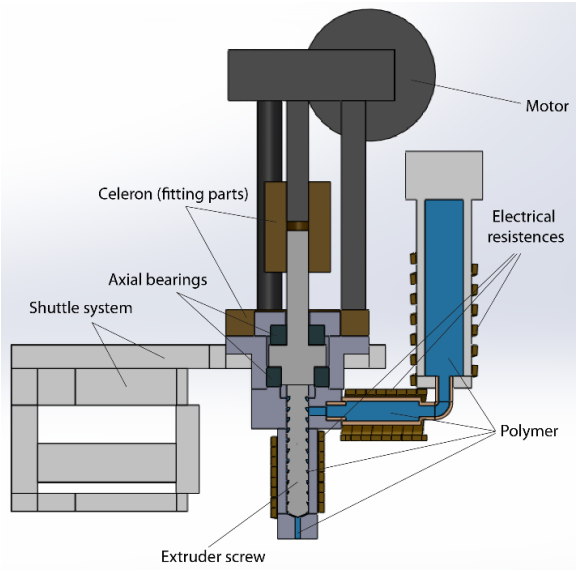

Fig. 5. Internal view of the extrusion system of the machine.

Also, the importance of the effects of radiation were considered by applying this condition to a closed group of surfaces, represented in the figure by the letter "B", containing the three electrical resistances exterior surfaces plus extrusion table and two lateral sheet metal inner surfaces. The emissivity ε depends on the surface material and finish. The values used in this work are listed in Table 2 [22].

Surface – Material	ε - Reference Temperature
Resistances – Stainless Steel	0.74 – 316 °C
Lateral metal sheets – Steel (Rolled)	0.66 - 21 °C
Extrusion base - acrylic	0.95 – 25 °C

Tab. 2. Total emissivity of materials subject to radiation during the simulation.

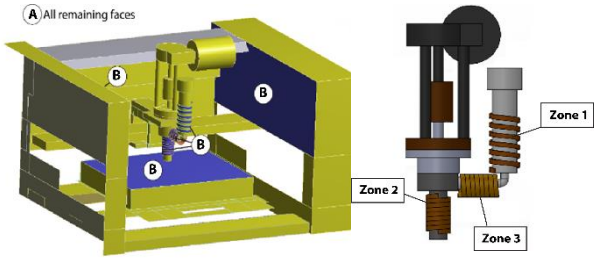

a) b)

Fig. 6. Boundary conditions applied to the ANSYS v15.0 FEA model: a) Letter "A" represents only convection condition, letter "B" represents applied radiation enclosures and convection, b) Indication of the three temperature zones.

One of the most important complaints was related to the regulation of the machine thermostats. The theoretical values states that those resistances need to be settled at 80ºC [20]. However, the laboratory technicians were checking that the resistance referred in Figure 6 as "Zone 3" – located at the horizontal polymer passage – needed to be, at least, settled at 90 º C to avoid the polymer premature solidification. Therefore, it was performed two configurations referred in this work, as *"80-80-80"* and *"80-80-90"*.

In terms of an ideal heating system, the machine resistances should become hot enough instantaneously. Nevertheless, the laboratory technicians estimated approximately 10 minutes until temperature stabilization in the machine, and also noticed that the machine thermostats doesn't heat in a gradual way, achieving temperatures as high as 190ºC before the complete stabilization, which could cause non expected heat transfer to the machine. In this case, a very realistic transient analysis was proposed, considering all temperature variation as shown by the thermostat screens, to the two configurations mentioned above.

Fig. 7 shows the machine thermostats, for the second configuration, after achieving its stabilization. Those measures were performed with the aid of a footage directed to the temperature displays, and then listed in a table to be embedded in the transient analysis setup.

Fig. 7. Thermostat system, settled for the configuration "80-80-90", after 8 minutes of footage.

V. Results

Fig. 8 shows the temperature variation. It is worth noting that the minimum temperature of the PCL for both cases stabilizes between 62 and 64 ºC, evidencing the possible occurrence of solidification of the polymer in regions of the screw that are more distant from the nozzle.

Due to the geometrical complexity, the region where the polymer meets the extrusion screw becomes a source of problems related to premature solidification of the polymer. Fig. 9 shows that an increase of the resistance temperature in "*Zone 3*" does not necessarily culminate in a better temperature control in that critical region, which can be seen as an increase of approximately 2 ºC at a cost of using extra 10ºC in the heat source.

The main problem with this approach is that other regions will suffer an undesirable increase temperature. Domingos, et al. [20] refers that, for this particular machine, an increase in the liquefier temperature from 80 to 100ºC corresponded to a considerable increase in terms of filament diameter, which reflects in a porosity decrease from 67 to 53 percent.

Considering that, it is desirable to prioritize the temperature uniformity over its increase in the critical regions and also that we must keep the changes within an acceptable limit of new investments, a third proposal was presented. By changing the material of the extrusion screw lower housing to aluminum alloy instead of the actual stainless steel, it become possible to see an actual improvement, since the thermal conductivity of aluminum alloy is approximately 10 times higher than the stainless steel.

A new transient simulation was performed considering this scenario, keeping the temperatures as initially desired. The results shows a better temperature distribution, with less than 4 ºC of difference between the colder and hotter regions. In addition, the critical region referred in Figure 10 can receive more conducted heat generated at *"Zone 2"* and *"Zone 3"*, keeping this point free of the premature solidification of the PCL.

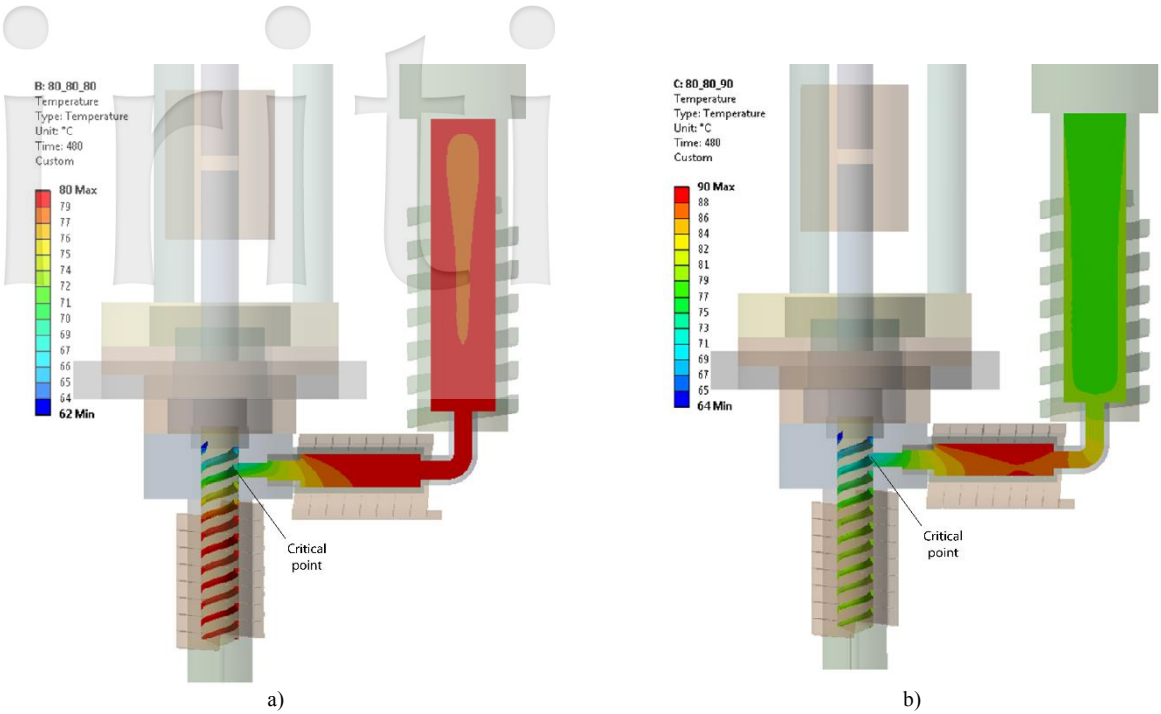

a) b)

Fig. 8. Temperature of the PCL after 480 s of transient analysis: a) case *"80-80-80"*, with a maximum of 80 and minimum of 62 ºC; b) case *"80-80-90"*, with a maximum of 90 and minimum of 64 ºC.

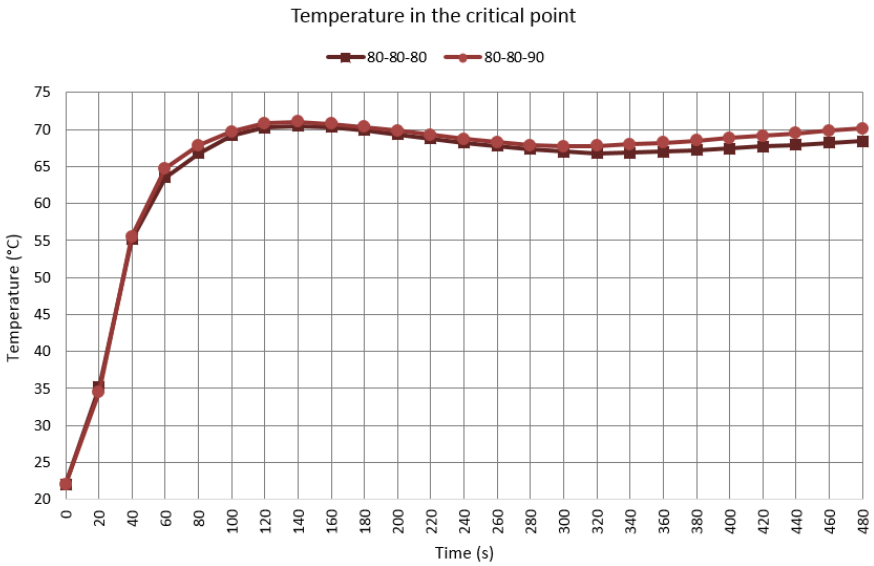

Fig. 9. Temperature variation in time of the PCL for both configurations.

An illustration of the changed part and the thermal behavior of the PCL achieved after that are shown in Fig. 10.

VI. Conclusions

In this paper, it is discussed one among various aspects regarded to the importance of the thermal behavior of a heat-based extrusion system. It aims to improve the temperature distribution using one of its most important base materials, the Polycaprolactone (PCL). Being guided by the parameters listed in a previous optimization study, as well as those found in a more practical way, it was defined two thermal configurations, named respectively as *"80-80-80"* and *"80-80-90"*. In both cases, it was shown that the polymer is not receiving the required amount of heat in some critical regions, which can compromise the entire precision of the extrusion process and/or introduce unpredicted thermal gradients. However, before propose an expensive change, a simple material substitution appears to be very promising, once that it can be possible to keep the entire PCL at a desired temperature.

Several other subjects can be discussed concerning the thermal behavior of the Bioextruder. Since this machine receives heat from three different sources, it is imperative to keep a good control of potential problems related to thermal expansion in regions with a need of higher accuracy.

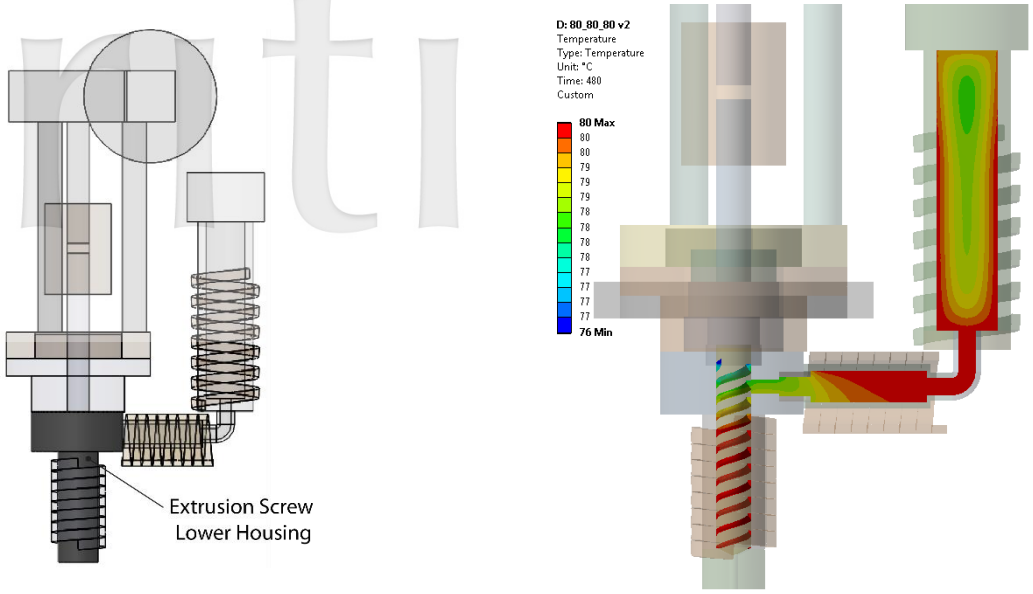

a) b)

Fig. 10. Theoretical improvement obtained by material replacement: a) Indication of the changed part, from stainless steel to aluminum alloy; b) Temperature distribution of the PCL after 480 seconds.

The Bioextruder is a very promising machine, with a wide variety of applications. It is undoubtedly a very interest study subject, helping it to become an excellent option in the precision 3D printing market.

VII. Acknowledgments

The authors would like to express their gratitude to the Centre for Rapid and Sustainable Product Development – CDRSP, to the Polytechnic Institute of Leiria – IPL, to the Center for Information Technology Renato Archer – CTI and to the University of Sao Paulo. This work was carried out with the grant supports from the Marie Curie funded project IREBID (FP7-PEOPLE-2009-IRSES-247476).

References

[1] Almeida, H. A., Bartolo, P. J., 2010. Virtual topological optimization of scaffolds for rapid prototyping. *Medical Engineering & Physics*, 32 (7), 775-782

[2] Hutmacher, D. W., 2000. Scaffolds in tissue engineering bone and cartilage. Biomaterials, 21 (24), 2529-2543.

[3] Lanza, R. L. and Vacanti, J. P. (Eds), 2013. Principles of Tissue Engineering, 4th ed. Elsevier Inc. ISBN: 978-0-12-398358-9.

[4] Liu, C., Xia, Z., Czernuszka, J. T., 2007. Design and development of three-dimensional scaffolds for tissue engineering. *Chemical Engineering Research and Design,* 85 (7), 1051-1064.

[5] Bose, S.; Roy, M., Bandyopadhyay, A., 2012. Recent advances in bone tissue engineering scaffolds. *Trends in Biotechnology*, 30 (10), 546-554.

[6] Zhang, Q., et al. 2014. Pore size effect of collagen scaffolds on cartilage regeneration. *Acta Biomaterialia*, 10 (5), 2005-2013.

[7] Gross, B. C., et al. 2014. Evaluation of 3D printing and its potential impact on biotechnology and the chemical sciences. *Analytical Chemistry*, 86, 3240-3253.

[8] Pepper, M. E. et al., 2009. Design and implementation of a two-dimensional inkjet bioprinter. *In: Proceedings of the 31st Annual International Conference of the IEEE EMBS*, 6001-6005, Minneapolis, MN.

[9] Inforçatti Neto, P. *et al*., 2014. Development of an interchangeable head based on variable section screw applied to desktop 3-D printers. In: Bartolo, P. J., et al. (Eds.), *High Value Manufacturing: Advanced Research in Virtual and Rapid Prototyping*, 19-23.

[10] Mironov, V., Kasyanov, V., Markwald, R. R., 2011. Organ printing from bioprinter to organ bio fabrication line. *Current Opinion in Biotechnology,* 22 (5), 667-673.

[11] Labet, M., Thielemans, W., 2009. Synthesis of polycaprolactone: a review. *Chemical Society Reviews*, 38 (12), 3484-3504.

[12] Wen, J., 2007. Heat Capacities of Polymers. *In: Mark, J. E. (Ed.). Physical properties of polymers handbook*, 2nd ed., Springer. 145-154.

[13] Gaur, U., Wunderlich, B. B., Wunderlich, B., 1983. Heat capacity and other thermodynamically properties of linear polymers. VIII. Polyesters and polyamides. *Journal of Physical and Chemical* Reference Data, 12 (29), 91-108.

[14] Cook, R., 1995. *Finite Element Modeling for Stress Analysis*. John Wiley & Sons, Inc. New York, NY. ISBN: 0471107743

[15] Bergman, T., et al., 2011. *Fundamentals of heat and mass transfer*, 7th ed. John Wiley & Sons, Inc. ISBN 13: 978-0470-50197-9

[16] Siegel, R.; Howell, J., 2002. *Thermal radiation heat transfer*, 4th ed, Taylor and Francis, New York.

[17] Bartolo, P. J., et al., 2012. Biomedical production of implants by additive electro-chemical and physical processes. *CIRP Annals-Manufacturing Technology*, 61 (1), 635-655.

[18] Domingos, M., et al., 2009. Polycaprolactone Scaffolds Fabricated via Bioextrusion for Tissue Engineering Applications. *International Journal of Biomaterials*, 2009, 9 pages.

[19] Mota, C. M. D., 2008. *Sistema de bioextrusão para engenharia de tecidos*. Mechanical engineering master's dissertation, University of Aveiro – Portugal, 111 pages.

[20] Domingos, M., et al., 2012. Effect of process parameters on the morphological and mechanical properties of 3D Bioextruded Poly (e-caprolactone) scaffolds. *Rapid Prototyping Journal*, 18, 56-67.

[21] Abdul-Jabbar, N. K., 2001. Natural convective heat transfer coefficient – a review I. Isolated vertical and horizontal surfaces. *Energy Conversion and Management*, 42 (4), 491-504.

[22] Mikron Instrument Company, Inc: Table of Emissivity of Various Surfaces for Infrared Thermometry. Web. 25 Feb. 2014, http://www-eng.lbl.gov/~dw/projects/DW4229_LHC_detector_analysis/calculations/emissivity2.pdf.

[23] Agarwal, R., et al., 2006. Thermal conduction and diffusion through polyesters composites. Council for Scientific and Industrial Research, 44 (10), 746-750.

[24] Perstorp Winning Formulas: CapaTM 6500 Datasheet. Web. 27 Dec. 2013. < https://www.perstorp.com/en/Products/Capa_6500>.

[25] Prospector Materials Database – UL IDES. Web. 03 Feb. 2014. http://plastics.ides.com/generics/37/c/t/polyester-properties-processing/sp/28.